CHINESE OPTICS LETTERS

Vol. 22, No. 7 | July 2024

Single-photon frequency-modulated continuous-wave Lidar based on quantum compressed sensing

Liu Yang (杨 柳)[1,2], Hongqi Niu (牛鸿琪)[1,2], Shuxiao Wu (吴舒啸)[1,2], Jianyong Hu (胡建勇)[1,2*], Mingyong Jing (景明勇)[1,2], Zhixing Qiao (乔志星)[3], Changgang Yang (杨昌钢)[1,2], Guofeng Zhang (张国峰)[1,2], Chengbing Qin (秦成兵)[1,2], Ruiyun Chen (陈瑞云)[1,2], Liantuan Xiao (肖连团)[1,2**], and Suotang Jia (贾锁堂)[1,2]

[1] State Key Laboratory of Quantum Optics and Quantum Optics Devices, Institute of Laser Spectroscopy, Shanxi University, Taiyuan 030006, China

[2] Collaborative Innovation Center of Extreme Optics, Shanxi University, Taiyuan 030006, China

[3] College of Medical Imaging, Shanxi Medical University, Taiyuan 030001, China

*Corresponding author: jyhu@sxu.edu.cn

**Corresponding author: xlt@sxu.edu.cn

Received January 11, 2024 | Accepted March 15, 2024 | Posted Online July 17, 2024

Frequency-modulated continuous-wave (FMCW) Lidar has the characteristics of high-ranging accuracy, noise immunity, and synchronous speed measurement, which makes it a candidate for the next generation of vehicle Lidar. In this work, an FMCW Lidar working at the single-photon level is demonstrated based on quantum compressed sensing, and the target distance is recovered from the sparse photon detection, in which the detection sensitivity, bandwidth, and compression ratio are improved significantly. Our Lidar system can achieve 3 GHz bandwidth detection at photon count rates of a few thousand, making ultra-long-distance FMCW Lidar possible.

Keywords: frequency-modulated continuous-wave Lidar; single-photon Lidar; quantum compressed sensing.
DOI: 10.3788/COL202422.072602

1. Introduction

Long-distance light detection and ranging (Lidar) has attracted significant attention in military, astronomical, and civil fields. Frequency-modulated continuous-wave (FMCW) Lidar[1-3] has significant advantages in high-ranging accuracy, noise immunity, fast-moving target capture, and synchronous speed measurement, compared with other Lidar technologies such as phased array Lidar, time-of-flight Lidar, and pulsed-light Lidar[4-8]. These advantages allow the technique to enable applications such as three-dimensional (3D) object profiling[9-11], synthetic aperture imaging Lidar[12,13], noncontact precision metrology[14], and swept-source optical coherence tomography[15].

However, at considerably great target distances, or in certain special scenarios, such as deep-space and deep-sea applications[16,17], the reflected probe beam attenuates to the single-photon level. Although a higher power local oscillator improves the signal-to-noise ratio (SNR) of the beat signal[18], long-distance detection requires a detection system capable of broadband measurements, and the bandwidth and the sensitivity are incompatible features for a coherent heterodyne detector. Geiger-mode single-photon detectors have been applied to coherent detection to reduce laser power[19]. Furthermore, data acquisition is restricted by the Nyquist–Shannon sampling theorem[20]. The photon counting technique is utilized for frequency recovery of the beat signal[21,22]. The amount of data to be processed is time consuming and memory intensive.

Compressed sensing (CS) can recover the sparse signals with a sampling rate much lower than the Nyquist sampling rate, promising real-time, broadband signal detection[23-26]. Generally, random sensing matrices are usually used for CS since they satisfy the restricted isometry property with a high probability. For a one-round FMCW Lidar measurement, a single range with a round-trip delay produces a single-frequency beat signal, which meets the requirements of the signal sparsity of CS. The 1-bit CS is utilized to recover the frequency of the beat signal from the photon arrival sequence[27]. Although it works, the 1-bit quantization method is not fully applicable to photon detection-based situations. In fact, randomness is a fundamental property in quantum mechanics. The quantum compressed sensing (QCS) method realizes compressed sampling of sparse signals in the transform domain by preparing and detecting quantum state processes. In our previous work, a broadband (>1 GHz) single-photon modulation spectrum measurement method was proposed and experimentally verified based on QCS[28-31].

In this work, FMCW Lidar working at the single-photon level is demonstrated based on QCS, in which the detection

sensitivity, bandwidth, and compression ratio (CR) are improved significantly. In the single-photon FMCW Lidar, the interference at the single-photon level leads to the probability modulation of photon detection. The QCS constructs the CS using quantum physical processes, enabling us to recover target distances from the sparse photon sequence. The system is highly sensitive and capable of broadband measurement, which enables a large dynamic range and high-precision Lidar. Meanwhile, sub-Nyquist sampling significantly reduces the pressure of data storage and processing. In the experiment, a 3 GHz measurement bandwidth was realized with a photon count rate of kilo counts per second (kcps), and the CR improved by three orders of magnitude compared with that of the conventional coherent detection.

2. Compressive Single-Photon FMCW Laser Ranging

For the FMCW Lidar, the theoretical limit of the ranging resolution is inversely proportional to modulation bandwidth. However, laser phase noise and frequency nonlinear modulation can cause the spectrum of the beat signal to spread out during the actual measurement. Therefore, the ranging resolution is determined by considering both the modulation bandwidth and full width at half maximum (FWHM) of the spectrum of the beat signal[10].

Remote and high-precision FMCW Lidar requires discrete single-photon signals to recover the broadband beat signal, as shown in Fig. 1. QCS is a technology that constructs a CS system to realize data compression and broadband signal reconstruction based on quantum physical processes. In this study, the QCS includes two steps: random compressed sampling and information recovery.

For sampling in QCS, the beat signal x is first mapped to a quantum state $|\alpha\rangle$, which is transformed to $|\alpha^x\rangle$. Therefore, the mathematical model of QCS can be expressed as

$$y' = \hat{A}|\alpha^x\rangle. \tag{1}$$

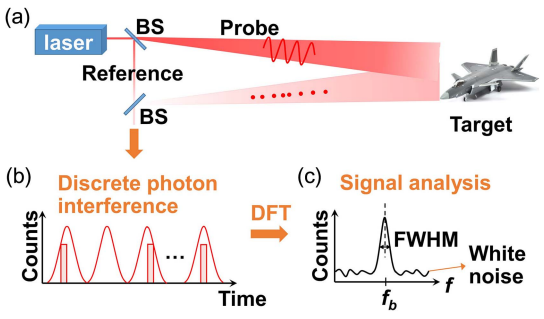

Fig. 1. Concept of the FMCW Lidar. (a) Schematic of the FMCW Lidar. (b) The compressed sampling of the random single-photon sequence. (c) The spectrum of the beat signal corresponding to the target distance is analyzed by the discrete Fourier transform (DFT). BS, beam splitter; FWHM, full width at half maximum.

Compared with the traditional CS system, in which the mathematical model is expressed as $y = Ax$, there are two major differences. First, the sensing matrix A is a random matrix for traditional CS; however, in QCS, it is replaced by a sensing operator $\hat{A}$. Secondly, the sensing matrix is predetermined and does not change with signals for traditional CS. As claimed in Ref. [29], the measurement process is non-adaptive[32]. However, the sensing matrix is related to the initial state $|\alpha\rangle$, the signal x, and the sensing operator $\hat{A}$, and it can only be determined when the measurement occurs for QCS, i.e., the quantum state collapse. Therefore, the measurement process in QCS is passive-adaptive, which is impossible with traditional electronic-based CS systems. In the process of QCS sampling, the frequency-modulated signal is first mapped to the photon wave function, making the probability of photon detection vary periodically. The second step is photon detection, which, according to quantum physical processes, causes the collapse of the quantum state. The probability of quantum measurement collapse is proportional to the square of the wave function amplitude. The high detection probability at the crest location and the low detection probability at the trough location allow the signal to be reconstructed with fewer photons. Then, a time domain signal of the random arrival of photons $[t_1, t_2, \ldots t_m]$ is collected, which is different from the time and amplitude information required in the traditional sampling.

In quantum mechanics, the intrinsic randomness stems from the consumption of coherence, which appears as white noise in the frequency domain, as shown in Fig. 1(c). We denote $|e_x, 0\rangle$ and $|e_y, 0\rangle$ as two orthogonal eigenstate vectors with the x-direction and y-direction of the laser. Similarly, we refer to $|e_x, 2\rangle$ and $|e_x, 1\rangle$ as the x-direction eigenstate vectors of the probe and reference beams, respectively, and denote $|e_y, 2\rangle$ and $|e_y, 1\rangle$ as the corresponding y-direction eigenstate vectors. Owing to the time delay between the frequency-modulated probe and reference beams, a relative phase difference φ is induced. The quantum-mechanical operator before the interference of the two beams is expressed as

$$\begin{aligned}\hat{\varphi}\hat{P}_{\mathrm{BS1}} = {} & |e_x, 1\rangle\langle e_x, 0| + |e_y, 1\rangle\langle e_y, 0| \\ & + \exp(i\varphi)|e_x, 2\rangle\langle e_x, 0| + \exp(i\varphi)|e_y, 2\rangle\langle e_y, 0|.\end{aligned} \tag{2}$$

The quantum-mechanical operator of the beat signal is expressed as

$$\begin{aligned}\hat{P}_{\mathrm{beat}} = \hat{P}_{\mathrm{BS2}}\hat{\varphi}\hat{P}_{\mathrm{BS1}} = {} & [1 + \exp(i\varphi)] \\ & \times (|e_x, 0\rangle\langle e_x, 0| + |e_y, 0\rangle\langle e_y, 0|).\end{aligned} \tag{3}$$

Therefore, the output state of the beat signal is determined solely by the relative phase difference φ. In the FMCW Lidar system, because φ is linearly frequency modulated, the probability of photon detection varies periodically.

For information recovery, the original beat signal x can be reconstructed with a high probability from a small number of measurements y by solving optimization problems[33,34].

Photon counting of the weak coherent state at the single-photon level obeys the Poisson distribution, i.e., the photon arrival time is completely random. The shot noise generated by the randomness of photon detection has the same power spectral density for each frequency component and shows as white noise in the frequency domain. The spectrum of the modulated weak coherent state is a superposition of white noise and the characteristic spectral line located at f_b. In this work, the single-photon beat signal is converted to the frequency domain using the DFT. The target distance R can be derived directly from the spectrum by locating the position of the characteristic spectral line. At this point, the compression measurement of the signal is completed. We did not finally recover the time domain waveform of the beat signal x because the purpose of this work is to obtain the distance information of the target, which can be obtained directly from the frequency of the beat signal; in fact, the time domain waveform can be obtained by a simple inverse Fourier transform of the spectrum. SNR of the spectrum is defined as

$$\mathrm{SNR} = 20\ \lg[V_{\max}/\mathrm{std}(V_{\mathrm{noise}})], \tag{4}$$

where $V_{\max}$ is the amplitude of the spectral peak and $\mathrm{std}(V_{\mathrm{noise}})$ is the standard deviation of the noise excluding the signal. The data CR could be defined as

$$\mathrm{CR} = C \times 32\,\mathrm{bit}/(f_b \times 12\,\mathrm{bit} \times 2) \times 100\%, \tag{5}$$

where C is the photon count per second, f_b is the bandwidth of the beat signal, and 32 bit and 12 bit are the resolutions of the compressed and classical sampling instruments, respectively.

The FMCW Lidar working at the single-photon level has been noticed and studied by several research groups. The signal reconstruction methods of these works are mainly divided into two kinds. One is the photon counting method[21,22,35], which first recovers the waveform through photon statistics and then performs fast Fourier transform (FFT) on the recovered waveform. The second is to utilize the traditional CS 1-bit quantization model to achieve signal recovery[27]. This method introduces the idea of binarization on the basis of traditional CS, i.e., the sampling results are quantized into 1 bit by setting a threshold. In contrast, the QCS method proposed in this paper utilizes the inherent randomness of quantum coherence measurement to achieve compressive measurements of the physical quantity being measured.

3. Experimental Setup

The single-photon FMCW Lidar system is shown in Fig. 2. A narrow linewidth external cavity tunable 1550 nm laser (Toptica) was selected as the light source. Pound–Drever–Hall (PDH) locking technology was used to lock the laser frequency to the reference frequency provided by the ultra-stable cavity to ensure the stability of the output frequency[36]. Linear frequency modulation was achieved using an electro-optic modulator and radio-frequency signal generator. Subsequently, the modulated laser was split into a probe and reference beam by a BS.

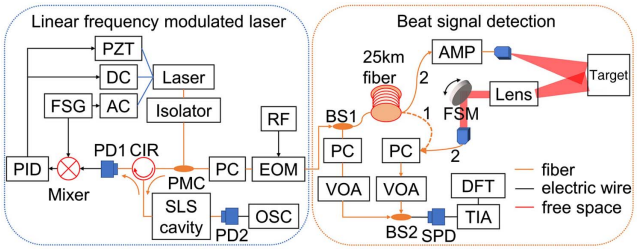

Fig. 2. The single-photon FMCW Lidar system. PID, proportional-integral-derivative; PZT, piezoelectric ceramic transducer; DC, direct current; AC, alternating current; FSG, function signal generator; CIR, circulator; PMC, polarization-maintaining coupler; PC, polarization controller; RF, radio frequency signal generator; EOM, electro-optic modulator; SLS cavity, ultra-stable cavity (SLS Company); OSC, oscilloscope; VOA, variable optical attenuator; PD, photoelectric detector; BS, 50/50 beam splitter; SPD, single-photon detector; TIA, time interval analyzer; AMP, amplifier; FSM, fast steering mirror.

The probe beam coherently interfered with the reference beam after covering a distance of 25 km. Here, the 25 km fiber is employed to emulate remote target detection, while simultaneously increasing the optical path difference between the signal light and reference light. This displacement effectively shifts the FMCW interference frequency from low to high frequencies, thereby circumventing low-frequency noise. An optical scanning system was added after 25 km fiber for 3D imaging. We first performed classical detection using a photodetector and a spectrum analyzer (ROHDE&SCHWARZ), combined with frequency locking to test the improvement in the ranging resolution. Furthermore, variable optical attenuators were used to simulate channel loss to the single-photon level. The beat signal was detected by a single-photon detector (IDQ230) with a high detection efficiency and low dark count rate, and the arrival time of each photon was recorded using a time interval analyzer (TIA, SIMINICS). The target distance was retrieved based on the post-processing QCS algorithm.

4. Experimental Results

By adding an optical scanning system to the system, targets at different positions are labeled with unique frequency shifts, and frequency mapping distance enables 3D reconstruction. In the experiment, the probe beam was coupled to the space through the 25 km fiber and illuminated the targets. Targets containing a plastic cube with a diameter of 2 cm, a regular hexagon, and an equilateral triangle with reflective tape were located at a distance of 1 m from the lens in the imaging system. The objects were separated by 5 and 7.5 cm as shown in Fig. 3(a). The optical scanning system consisted of a 4f system and a fast steering mirror to detect illuminated objects for reconstructing 57 pixel × 21 pixel resolution depth map and 3D imaging. Figure 3(b) shows the two-dimensional (2D) reconstruction from the frequency of the beat signal, and the 3D reconstruction of the target is shown in Fig. 3(c). To accelerate the imaging time, the dead time of the detector was set to

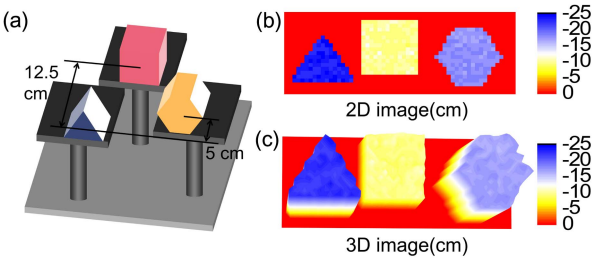

Fig. 3. 3D image of target. (a) The target containing multiple objects. (b) The 2D reconstruction. (c) The 3D image according to the frequency mapping distance.

2 μs. The photon intensity of the reference path was maintained at 90 kcps, and the photon intensity of the probe path was collected at 50–110 kcps due to the different reflectivity of the objects. Two seconds of photon signals were accumulated on each pixel. The beat signal was averaged 8 times to improve the SNR. To ensure the SNR of the beat signal in single-photon coherent detection, the photon intensity of the reference and the signal paths should be equal. The optimal solution in scanning imaging is that the photon intensity of the reference path needs to be adaptively and optimally adjusted at each pixel point. We do not change the photon intensity of the reference path in our experiments, which is universal in real-world environments.

4.1. Analysis of range resolution and accuracy

Since imaging resolution is related to frequency resolution, we investigated and analyzed factors that affect frequency resolution and accuracy, such as frequency modulation linearity, detection range, sweep rate, and bandwidth. Figures 4(a) and 4(b) show a comparison of the spectrum of the beat signal with and without frequency locking for the classical detection. The spectrum of the beat signal was measured with a linear frequency modulation sweep rate of 4 Hz and a sweep bandwidth of 3.3 GHz. The measured signals were averaged 200 times to improve the SNR. The phase noise of the free-running laser causes spectral broadening of the beat signal. The long-range transmission also introduces phase noise, which widens the FWHM of the spectrum of the beat signal to 65,844 Hz. However, the phase noise can be suppressed well, and the FWHM can be narrowed to 9.09 Hz with frequency locking. Accordingly, the frequency noise was suppressed by approximately 40 dB, which significantly improved the frequency resolution of the beat signal.

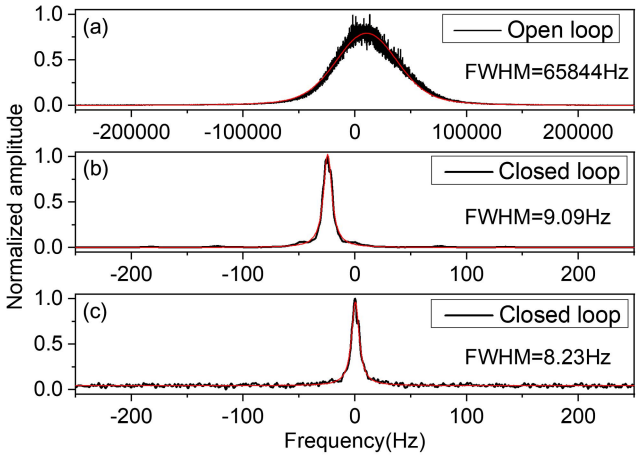

Fig. 4. The spectrum of the beat signal when the laser is running freely and when the closed-loop frequency locking system is employed. The graph is centered on the frequency of 1,620,173 Hz. The black line is the experimental result and the red line is curve fitting. (a) Open-loop operation and classical detection. (b) Closed-loop operation and classical detection. (c) Single-photon detection and closed-loop operation.

The spectrum of the beat signal for the single-photon detection is shown in Fig. 4(c), with the spectral FWHM of 8.23 Hz by frequency locking. In this experiment, the mean photon count rate of the beat signal was ~8 kcps and data for 1000 s were collected to improve the SNR. The photon sequence recorded by the time interval analyzer is divided into segments, and each segment is processed using the DFT algorithm[29-31,37]. Because the center frequency of the spectrum of the beat signal is approximately 1.62 MHz, and the photon count is merely 8 kcps, the data CR is 6.58×10^{-3} according to the sampling theorem. The spectral SNR is 37.90 dB.

However, when fewer photons are detected, the quantum shot noise dominates, which appears as white noise in the frequency domain. Consequently, the SNR of the spectrum decreases. It is worth highlighting that the FWHM in single-photon detection is identical to that in classical detection. Clearly, QCS technology maintains the range resolution despite a reduction in the average photon count and enables high-precision long-range detection. Importantly, the 27 Hz shift in the peak signals of the classical and single-photon measurements is caused by the different reference clocks of the measuring instruments.

The relationship between the FWHM of the spectrum of the beat signal and the target distance with different sweep rates is shown in Fig. 5(a) for a sweep bandwidth of 3.3 GHz. We measured the beat signal at the range of 1–12.5 km, and added 20, 25, 30, 30.5, 32.5, and 40 cm to the 12.5 km optical fiber. As the fiber length is further expanded, phase noise caused by temperature drift and mechanical vibration cannot be ignored. The Doppler noise caused by the stress and strain of the fiber results in phase or frequency variations of the transmitted signal. The FWHM of the beat signal at a 12.5 km distance is nearly twice as large as that at a 1 km distance. Similarly, the FWHM of the beat signal exceeded 1 Hz at a sweep rate of 1 Hz owing to the phase noise of the system. After several measurements, the minimum of the FWHM of the beat signal is 2.18 Hz at a sweep rate of 1 Hz. In addition, when the sweep rate is 4 Hz, double peaks occasionally appear in the spectrum when the distance is 12.504 km, as shown in Fig. 5(b), owing to the frequency shift of the beat signal caused by the Doppler noise. The spectral SNR is reduced to 35.50 dB. The maximum of the FWHM of the spectrum is 8.83 Hz at a sweep rate of 4 Hz, and the corresponding ranging

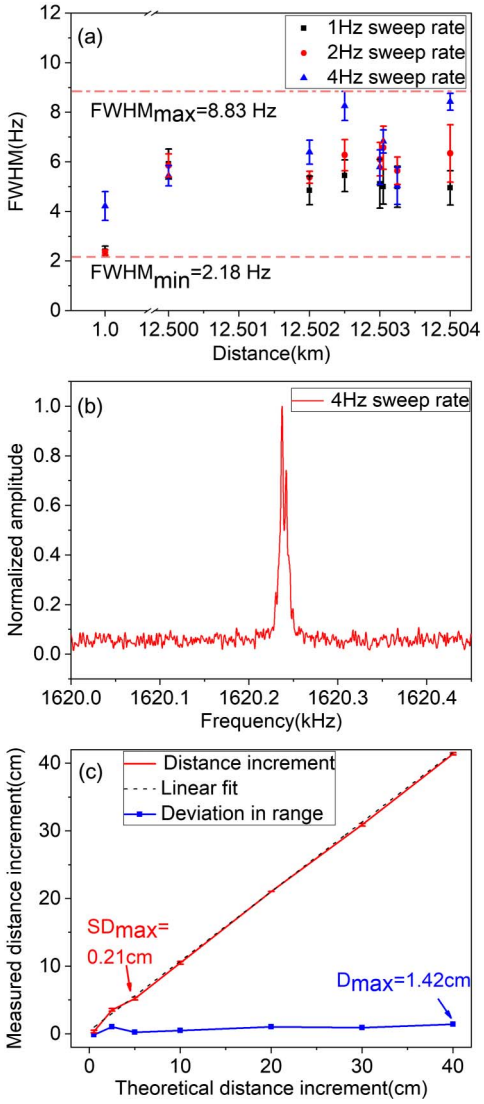

Fig. 5. The ranging resolution and accuracy. (a) The FWHM of the spectrum of the beat signal with different target distances and different sweep rates. (b) The spectrum of the beat signal has double peaks because of the frequency shift of the beat signal caused by the Doppler noise of the fiber. (c) The relationship between the measured and theoretical distance increments. The linear fitting slope of the experimental data is 1.02.

resolution is 6.69 cm, which is twice the theoretical limit of ranging resolution.

To further illustrate the ranging resolution and accuracy of the system, the distance increments of 0.5, 2.5, 10, 20, 30, and 40 cm were used as shown in Fig. 5(c), with a sweep rate of 4 Hz and a sweep bandwidth of 3.3 GHz. The result shows that the deviations between the experimental and theoretical values are 1.05 and 0.23 cm when the distance shift is 2.5 and 5 cm, respectively. The experimental system could distinguish a distance increment of 5 cm. Error bars were obtained by taking multiple measurements of the frequency of the beat signal for each distance. The maximum value of the error bar is

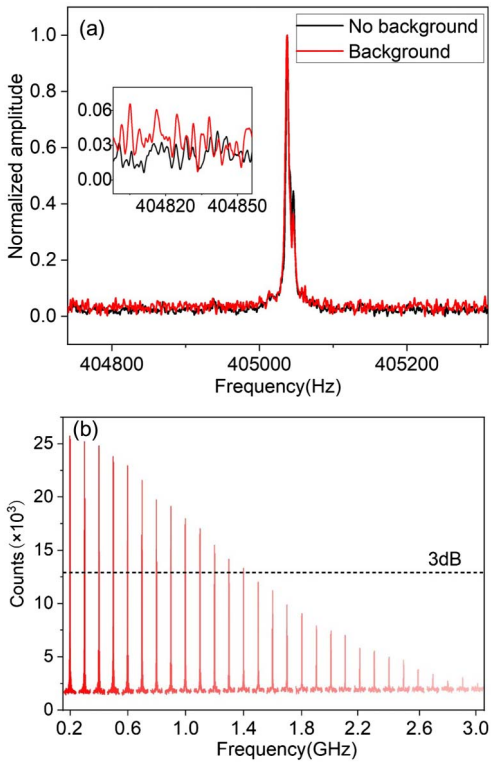

Fig. 6. Noise immunity and broadband detection of our proposal. (a) Comparison of the spectra of the beat signals with and without background noise. (b) Test of broadband detection capability of our system from 200 MHz to 3 GHz based on QCS technology.

0.28 Hz, indicating that the ranging accuracy of the system is 0.21 cm.

4.2. Noise immunity and broadband detection

FMCW Lidar is immune to ambient noise since the background noise photons are incoherent with the modulated beam. With the proposed QCS, our experiment shows that FMCW Lidar is also applicable at the single-photon level. In the experiment, an additional 1550 nm laser beam was added to the probe beam as background noise. The noise, probe, and reference beam photon count rate were all 6 kcps. Figure 6(a) shows a comparison of the spectra of the beat signals with and without background noise at a linear frequency modulation sweep rate of 1 Hz and a sweep bandwidth of 3.3 GHz; the frequency of the beat signal is 405,037.6 Hz, corresponding to the target distance of 12.53971 km. The signal and background noises can still be clearly distinguished, which can be attributed to the fact that the background noise without frequency modulation has the same power spectral density in each frequency component. The FWHM remains almost unchanged with and without the background noise. The spectral SNR is reduced from 41.30 to 38.54 dB due to the addition of background noise. A relatively higher SNR = 41.30 dB is acquired in quieter experimental environments and with better visibility of the interference of optical

coherence. In addition, 1000 s data accumulation is used to show better spectral SNR. Under the condition that the noise intensity is the same as the signal beam intensity, theoretically 2000 photons can recover the spectrum. Our experimental system is not only suitable for long-distance high-sensitivity detection but also for environments containing strong background noise.

In the FMCW Lidar, the measurable bandwidth determines the range and resolution of the system. To demonstrate the broadband measurement capability of our system, the laser was frequency-modulated by applying signals of different frequencies to the electro-optic modulator. Photon detection and frequency demodulation were performed based on the QCS technique, and the results are shown in Fig. 6(b), where the frequency varies from 200 MHz to 3 GHz. The results show that the 3 dB bandwidth of the system is 1.43 GHz when the photon counting rate is approximately 6.8 kcps and the data compression rate reaches 6.34×10^{-6}. The measurement bandwidth of 1.43 GHz theoretically corresponds to 10,800 km of range length with a sweep rate of 4 Hz and a sweep bandwidth of 3.3 GHz. With the measurement sensitivity, bandwidth, and CR significantly improved, our results represent significant progress toward practical ultra-long-range Lidar.

5. Conclusion

In this study, FMCW Lidar working at the single-photon level is demonstrated based on QCS, in which the detection bandwidth and CR are improved significantly. QCS constructs the CS using quantum physical processes, enabling us to recover target distances from the discrete random single-photon sequence. Moreover, the system is highly sensitive and capable of broadband measurement, which enables a large dynamic range and high-precision Lidar. Meanwhile, sub-Nyquist sampling significantly reduces the data size and the pressure of data storage and processing. In the experiment, a 3 GHz measurement bandwidth was realized with a photon count rate of kcps, and the CR improved by three orders of magnitude compared with that of conventional coherent detection. To further improve the ranging resolution, the tunable laser was locked to an ultra-stable cavity using frequency locking technology, and the linewidth of the laser was narrowed to the Hz level, which overcomes the range limitation owing to the laser coherence length. Our proposal provides an idea for the application of QCS and solves the bottleneck problem of FMCW Lidar technology, which will greatly expand its applications in deep space, underwater, and harsh environments.

Acknowledgements

This work was supported by the National Natural Science Foundation of China (Nos. 62105193, 62127817, 62075120, 62075122, U22A2091, 62222509, 62205187, and 62305200), the Shanxi Province Science and Technology Major Special Project (No. 202201010101005), the National Key Research and Development Program of China (No. 2022YFA1404201), the Program for Changjiang Scholars and Innovative Research Team in University (No. IRT_17R70), the China Postdoctoral Science Foundation (No. 2022M722006), the Shanxi Province Science and Technology Innovation Talent Team (No. 202204051001014), the Science and Technology Cooperation Project of Shanxi Province (No. 202104041101021), and the Shanxi "1331 Project" and 111 Project (No. D18001). J. Hu and L. Xiao proposed the research. L. Yang performed the experiment and analyzed the data with the help of J. Hu, M. Jing, and Z. Qiao. S. Wu helped with the data acquisition. All authors contributed to writing this paper.

References

1. E. W. Mitchell, M. S. Hoehler, F. R. Giorgetta, *et al.*, "Coherent laser ranging for precision imaging through flames," Optica **5**, 988 (2018).
2. P. Feneyrou, L. Leviandier, J. Minet, *et al.*, "Frequency-modulated multifunction lidar for anemometry, range finding, and velocimetry-1. Theory and signal processing," Appl. Opt. **56**, 9663 (2017).
3. S. Kakuma, "Frequency-modulated continuous-wave laser radar using dual vertical-cavity surface-emitting laser diodes for real-time measurements of distance and radial velocity," Opt. Rev. **24**, 39 (2017).
4. C. P. Hsu, B. Li, B. Solano-Rivas, *et al.*, "A review and perspective on optical phased array for automotive LiDAR," IEEE J. Sel. Top. Quantum Electron. **27**, 1 (2021).
5. C. V. Poulton, A. Yaacobi, D. B. Cole, *et al.*, "Coherent solid-state LIDAR with silicon photonic optical phased arrays," Opt. Lett. **42**, 4091 (2017).
6. Y. S. Jiang, S. Karpf, and B. Jalali, "Time-stretch LiDAR as a spectrally scanned time-of-flight ranging camera," Nat. Photonics **14**, 14 (2020).
7. S. Chan, A. Halimi, F. Zhu, *et al.*, "Long-range depth imaging using a single-photon detector array and non-local data fusion," Sci. Rep. **9**, 8075 (2019).
8. R. Horaud, M. Hansard, G. Evangelidis, *et al.*, "An overview of depth cameras and range scanners based on time-of-flight technologies," Mach. Vis. Appl. **27**, 1005 (2016).
9. D. J. Lum, S. H. Knarr, and J. C. Howell, "Frequency-modulated continuous-wave LiDAR compressive depth-mapping," Opt. Express **26**, 15420 (2018).
10. R. K. Ula, Y. Noguchi, and K. Iiyama, "Three-dimensional object profiling using highly accurate FMCW optical ranging system," J. Lightwave Technol. **37**, 3826 (2019).
11. Z. P. Li, J. T. Ye, X. Huang, *et al.*, "Single-photon imaging over 200 km," Optica **8**, 344 (2021).
12. G. Z. Li, R. Wang, Z. Q. Song, *et al.*, "Linear frequency-modulated continuous-wave ladar system for synthetic aperture imaging," Appl. Opt. **56**, 3257 (2017).
13. G. Z. Li, Z. H. Zhang, Y. F. Zhang, *et al.*, "Estimation and correction of vibration-induced range cell migration for FMCW synthetic aperture ladar," Appl. Opt. **59**, 2874 (2020).
14. A. B. Mateo and Z. W. Barber, "Multi-dimensional, non-contact metrology using trilateration and high resolution FMCW ladar," Appl. Opt. **54**, 5911 (2015).
15. D. Huyan, N. Lagrosas, and T. Shiina, "Target imaging in scattering media using ghost imaging optical coherence tomography," APL Photonics **7**, 086104 (2022).
16. R. W. Lee, A. Laux, and L. J. Mullen, "Hybrid technique for enhanced optical ranging in turbid water environments," Opt. Eng. **53**, 051404 (2014).
17. J. Heidemann, M. Stojanovic, and M. Zorzi, "Underwater sensor networks: applications, advances and challenges," Philos. Trans. R. Soc. London, Ser. A **370**, 158 (2012).
18. Z. W. Barber, J. R. Dahl, T. L. Sharpe, *et al.*, "Shot noise statistics and information theory of sensitivity limits in frequency-modulated continuous-wave ladar," J. Opt. Soc. Am. A **30**, 1335 (2013).
19. L. A. Jiang and J. X. Luu, "Heterodyne detection with a week local oscillator," Appl. Opt. **47**, 1486 (2008).
20. H. Nyquist, "Certain topics in telegraph transmission theory (Reprinted from Transactions of the A. I. E. E., February, pg. 617-644, 1928)," Proc. IEEE **90**, 280 (2002).

21. J. X. Luu and L. A. Jiang, "Saturation effects in heterodyne detection with Geiger-mode InGaAs avalanche photodiode detector arrays," Appl. Opt. **45**, 3798 (2006).
22. B. I. Erkmen, Z. W. Barber, and J. Dahl, "Maximum-likelihood estimation for frequency-modulated continuous-wave laser ranging using photon-counting detectors," Appl. Opt. **52**, 2008 (2013).
23. L. Z. Xue and H. Zou, "Sure independence screening and compressed random sensing," Biometrika **98**, 371 (2011).
24. E. J. Candes and M. B. Wakin, "An introduction to compressive sampling," IEEE Signal Process. Mag. **25**, 21 (2008).
25. G. A. Howland, D. J. Lum, M. R. Ware, *et al.*, "Photon counting compressive depth mapping," Opt. Express **21**, 23822 (2013).
26. S. Liu and Y. Chen, "Sub-Nyquist radar receiver based on photonics-assisted compressed sensing and cascaded dictionaries," Chin. Opt. Lett. **22**, 013902 (2024).
27. Z. Chen, B. Liu, G. M. Guo, *et al.*, "Photon counting heterodyne with a single photon avalanche diode," IEEE Photon. Technol. Lett. **33**, 931 (2021).
28. J. Y. Hu, M. Y. Jing, G. F. Zhang, *et al.*, "Performance of single-photons communication using the multi-channel frequency coding scheme," Opt. Express **26**, 20835 (2018).
29. J. Y. Hu, Y. Liu, L. L. Liu, *et al.*, "Quantum description and measurement for single photon modulation," Photonics Res. **3**, 24 (2015).
30. J. Y. Hu, B. Yu, M. Y. Jing, *et al.*, "Experimental quantum secure direct communication with single photons," Light Sci. Appl. **5**, e16144 (2016).
31. H. T. Zhou, C. B. Qin, S. P. Han, *et al.*, "Visualizing quantum coherence based on single-molecule coherent modulation microscopy," Nano Lett. **21**, 1477 (2021).
32. D. L. Donoho, "Compressed sensing," IEEE Trans. Inf. Theor. **52**, 1289 (2006).
33. R. G. Baraniuk, "Compressive sensing," IEEE Signal Process. Mag. **24**, 118 (2007).
34. M. F. Duarte and R. G. Baraniuk, "Spectral compressive sensing," Appl. Comput. Harmon. Anal. **35**, 111 (2013).
35. X. Huang, Y. Hong, Z. P. Li, *et al.*, "Frequency-modulated continuous-wave 3D imaging with high photon efficiency," Opt. Lett. **47**, 3568 (2022).
36. E. D. Black, "An introduction to Pound-Drever-Hall laser frequency stabilization," Am. J. Phys. **69**, 79 (2001).
37. J. Y. Hu, L. Yang, S. X. Wu, *et al.*, "Security proof of the two-way quantum secure direct communication with channel loss and noise," Europhys. Lett. **129**, 10004 (2020).